KNOW-BLADE Task-2 report: Aerodynamic accessories

Johansen, J.; Sørensen, Niels N.; Zahle, Frederik; Kang, S.; Nikolaou, I.; Politis, E.S.; Chaviaropoulos, P.K.; Ekaterinaris, J.

Publication date:
2004

Document Version
Publisher's PDF, also known as Version of record

RISØ

Risø-R-1482(EN)

KNOW-BLADE Task-2 report; Aerodynamic Accessories

Jeppe Johansen, Niels N. Sørensen, Frederik Zahle, Shun Kang, Ilias Nikolaou, Evangelos S. Politis, Panagiotis K. Chaviaropoulos and John Ekaterinaris

Risø National Laboratory
Roskilde
Denmark
October 2004

Author: Jeppe Johansen, Niels N. Sørensen, Frederik Zahle, Shun Kang, Ilias Nikolaou, Evangelos S. Politis, Panagiotis K. Chaviaropoulos and John Ekaterinaris
Title: KNOW-BLADE Task-2 report; Aerodynamic Accessories
Department: Wind Energy Department

Risø-R-1482(EN)
November 2004

Abstract (max. 2000 char.):

In the EC project KNOW-BLADE a work package has been defined to investigate the possibility to numerically model aerodynamic accessories in existing Navier-Stokes solvers. Four different aerodynamic accessories have been investigated.

Firstly, the potential of applying active flow control by means of a pulsating jet placed at the leading edge in order to enhance mean lift. The general trend is that increased pulsation frequency is beneficial, in that it reduces the oscillation amplitude and raises the mean lift level while lowering the mean drag level. An increased jet exit velocity has a tendency to increase the oscillation amplitude, which is not very attractive for load control on wind turbines.

Secondly, the effect of vortex generators has been modelled using two phenomenological vortex generator models. The models have been applied to three airfoil configurations. For all cases investigated the models shows qualitatively the correct behaviour, even though there are a considerable spread in the degree of success.

Thirdly, the influence of adding a stall strip for changing the airfoil characteristics was investigated. Stall strips at three different positions were directly modelled by changing the airfoil geometry. In general the 7mm stall strips placed at P00 and P-02 had the greatest effect on the max lift followed by stall strip P02. Unfortunately, there was not sufficient agreement between the experimental results and the simulations to draw any conclusions of optimum position and geometry of the stall strip.

Finally, the effect of surface roughness was modelled by either modifying the boundary condition of the turbulence model or by modifying the airfoil geometry. Using the roughness model gave relatively good agreement with measurements and it must be concluded that the effect of using roughness tape can be better predicted with a roughness model compared to using a modified airfoil surface.

ISSN 0106-2840
ISBN 87-550-3379-2(internet)

Contract no.:
ENK6-CT2001-00503

Group's own reg. no.:
1110033-00

Sponsorship:

Cover :

Pages: 31
Tables: 3
References: 33

Risø National Laboratory
Information Service Department
P.O.Box 49
DK-4000 Roskilde
Denmark
Telephone +45 46774004
bibl@risoe.dk
Fax +45 46774013
www.risoe.dk

Contents

Preface

The present work is made during the KNOW-BLADE EC project (contract number: ENK6-CT-2001-00503) in which nine partners are involved. These are:

Risø National Laboratory, Roskilde Denmark,	RISOE (Coordinator)
Centre for Renewable Energy Sources, Greece,	CRES
Deutches Zentrum fuer Luft- und Raumfahrt, Germany	DLR
Danmarks Tekniske Universitet, Denmark	DTU
Swedish Defence Research Agency, Sweden,	FOI
National Technical University of Athens, Greece	NTUA
Vrije Universiteit Brussels, Belgium	VUB
Foundation of Research and Technology, Greece	FORTH
LM Glasfiber A/S, Denmark	LMG

The main objective of the project is through research activities to fill in important knowledge gaps in the wind turbine community by applying Navier-Stokes (NS) solvers to a series of unsolved aerodynamic and aeroelastic problems. The present report describes the work carried out in work package WP2: Aerodynamic accessories in which RISOE, FORTH, CRES, DLR, VUB, DTU and LMG are involved.

In connection with modern wind turbines a series of different aerodynamic accessories or devices are used for adjusting the aerodynamic and aeroelastic behaviour of wind turbine blades. Typical applications are to adjust the power or the loads of the turbine, or to prevent undesired vibrations or multileveled power curves. Several devices are frequently applied; of these the most widely used are stall-strips, vortex generators and trip-tape/zig-zag tape. Stall-strips can be applied to control both the power and loads. Typically, these are mounted on the outer part of the blades to stabilize the flow by fixing the separation point. This will eventually cause reduced loads and lower power. Vortex generators are another type of device that can be used to control the loads and the power. These are typically applied on the inner part of the blades increasing the maximum lift by delaying separation on the airfoil suction side to higher incidences. Trip-tape or zig-zag taper are often used to assure that transition from laminar to turbulent flow takes place at the leading edge of the blades, securing that the turbine will operate on a given power curve and not fluctuate due to changes in the transition location. In the EC project KNOW-BLADE a work package was defined to investigate the possibility to numerically model aerodynamic accessories in existing Navier-Stokes solvers.

Often these aerodynamic devices are used to alter undesired behaviour for existing blades, fitting the devices based on experience and trial and error. Even though much experience has been acquired in industry and some amount of experimental data exist for these devices, the situation are far from optimal. It would be desirable to have the capabilities to accurately predict the changes in airfoil characteristics, i.e. lift and drag coefficients, using aerodynamic codes. This predictive capability would allow designers to work with the devices already during the design phases, and it would shorten the time spent when correcting existing designs.

In addition to the traditional accessories discussed above, it was decided to perform some initial investigations of a synthetic jet actuator, a so-called active flow control devices. These issues will be described Section 1. Section 2 deals with the modelling of vortex generators, while the modelling of stall strips is described in Section 3. Finally Section 4 describes the modelling of surface mounted trip tape.

1 Active Flow Control

Establishment of active or passive control of the flow over turbomachinery and rotor blades has been a continuous effort of experimental and theoretical investigation for the past decades. Numerous experimental investigations [1,2,3,4,5,6,7] and [8] have tested passive and active flow control concepts. It has been demonstrated that its application can yield significant improvements in aerodynamic performance. For example, Chang et al. demonstrate that flow separation over airfoils at high incidence can be successfully suppressed by high frequency transverse velocity fluctuations generated by acoustic excitations. More recently, refs [9] and [10] control of separated flows with pulsating jets yielded very encouraging results. Advances in "smart", compact flow actuation devices, such as synthetic jets [11] opened new horizons in flow actuation and can lead to significant improvements in aerodynamic performance of existing configurations. An extensive review of the techniques for manipulation of flow separation can be found in[12]. Among them steady blowing or suction [13] have shown promise to control separated flow over wings. The new active flow actuation methods and have the advantage that they require significantly less power input and introduce smaller design complexities. For example, the innovative method of flow control with synthetic jets requires only electric power and produces a high frequency pulsating jet with zero net mass input. It has been also demonstrated and that pneumatic flow control with pulsating jets can yield large improvements in performance with a small jet output rate. It has been demonstrated that oscillatory blowing is more effective than steady blowing in controlling boundary layer separation. This active flow control improves dynamic airfoil performance by eliminating large excursions in lift, drag, and pitching moment.

Numerical prediction of the beneficial effects of flow control reported in experimental studies was the subject of the investigation by Wu et al. [14] where flow control was simulated by a pulsating jet, which was located at quarter chord, and blowing was prescribed in the normal to the airfoil surface direction. It was found that lift increase in the post-stall regime could be achieved as was reported in the experiments. The effectiveness of a pulsating jet located at the leading edge of a NACA-0015 airfoil to control static stall was also investigated in the numerical investigation of Rao et al. . Hassan [15] and [16] investigated the effectiveness of a jet located at 0.13 % chord to control flow separation using Navier-Stokes methods and reported that a high jet momentum is needed to obtain a significant lift increase. In the numerical study of Donovan et al. [17] simulations of steady and pulsating jet flow controls were shown. McCormick developed a new concept for boundary layer separation control, the so-called "directed synthetic jet". The blowing slot of this jet is curved in the downstream direction. The jet energizes the boundary layer and makes it, in the time average, more resistant to separation. Synthetic jet flow control devices, refs. and , on the other hand, use membranes or springboards which are driven at resonance piezoelectrically or mechanically by motors and enhance the momentum of boundary layer by zero mass vortical flow. Synthetic jets were successfully used to control flow separation of low Reynolds number incompressible flows .

Further demonstration of the ability of pneumatic flow control to improve aerodynamic performance of high Reynolds number incompressible and compressible unsteady flows and dynamic stall is needed. To date, there are no analytical tools available to determine the range of parameters, such as jet location and speed or momentum coefficient and

pulsation frequency, for which flow control methods are most effective. As a result, for every new airfoil shape at fixed incidences, or for pitching airfoils with different unsteady parameters, such as oscillation amplitude or rate, the flow actuation parameters are determined heuristically.

1.1 Flow Control Parameters

It was demonstrated in the experiments and that the important parameters for airfoil flow control with pulsating jets are (1) the reduced excitation frequency, $F^+= c\ f_J /U_\infty$where c is the airfoil chord and f_J is the jet pulsation frequency, and (2) the oscillatory blowing momentum coefficient, $C_\mu = <J>/cq$, where $q=0.5\rho\ U_\infty^2$, <J> is the oscillatory momentum $<J>=\rho V_J\ H_J$,. H_J is the jet slot width, and V_J is the jet velocity oscillation amplitude.

The numerical simulations are fully turbulent since the step at the leading edge (see Figure 1) is expected to promote rapid transition to fully turbulent flow. The Reynolds number and the other flow parameters match the parameters of the measurements by Seifert et al. . Numerical simulations of pulsating jet flow control, where the jet exit velocity or momentum coefficient C_μ or the excitation frequency F^+ is a free parameter, are carried out. The objective of this investigation is to demonstrate that numerical solutions can be used to perform a sensitivity analysis of flow control parameters.

1.2 Methodology

Two different Navier-Stokes flow solvers were applied to the problem. The first is the flow solver of FORTH-IACM, [18] and [19] based on the pseudo compressible or artificial compressibility method and using the Spalart-Allmaras turbulence model. The second is the flow solver of RISOE and DTU, EllipSys2D [20,21] and [22] based on the pressure correction method using the k-ω SST turbulence model. Both methods are second order accurate in both time and space.

1.3 Meshes

Several different mesh topologies were tested, three of these are shown in Figure 1. The upper left picture shows an overview of the C-meshes used around the airfoil. The upper right picture shows a detail of a mesh where the surface geometry has been smoothed around the step. In the lower pictures details of meshes that resolves the step geometry are shown, the left mesh uses a single block construction while the mesh in the right mesh uses a two-block construction. For the passive case, where no jet actuation is present, the results obtained using the different mesh topologies showed minimal differences, and the remaining part of the investigation were performed on meshes of the two block configuration shown in lower right corner of the figure.

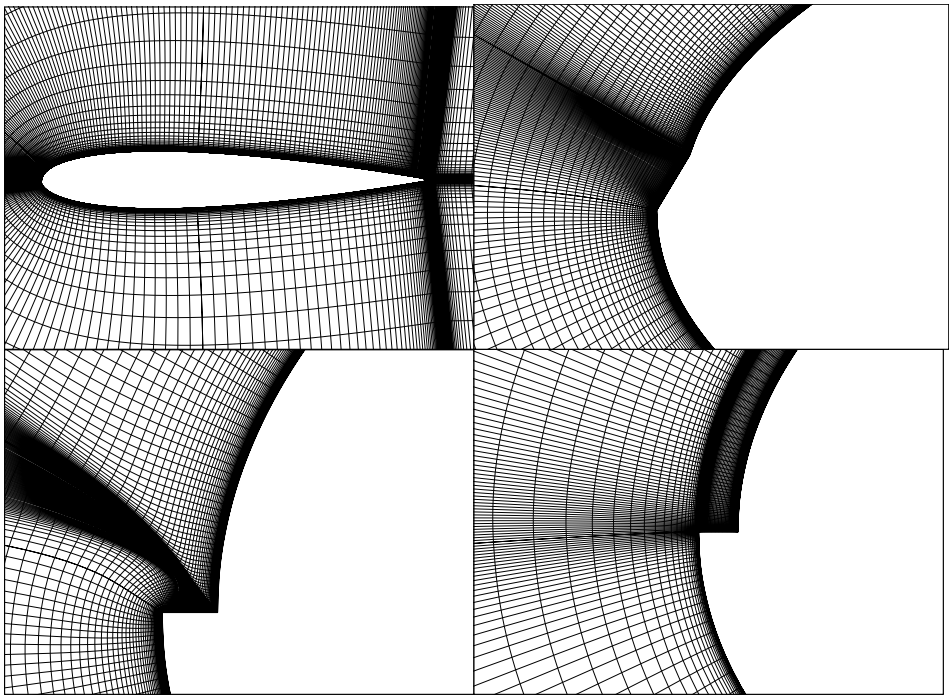

Figure 1: Grid around the leading edge of TAU-0015 airfoil, showing three different ways of resolving the region around the jet exit.

1.4 Time step investigation

The effect of changing the time-step was investigated for the active flow cases, where the time-step requirement is more restrictive than for the passive case. For one of the active flow control cases the time-step was varied between $\Delta t\ U_\infty / c = 1 \cdot 10^{-3}$ to $1.25 \cdot 10^{-4}$ to find the necessary time resolution, see Figure 2. From this investigation it could be concluded that for a dimensionless time-step less than $5 \cdot 10^{-4}$ a time independent solution could be obtained.

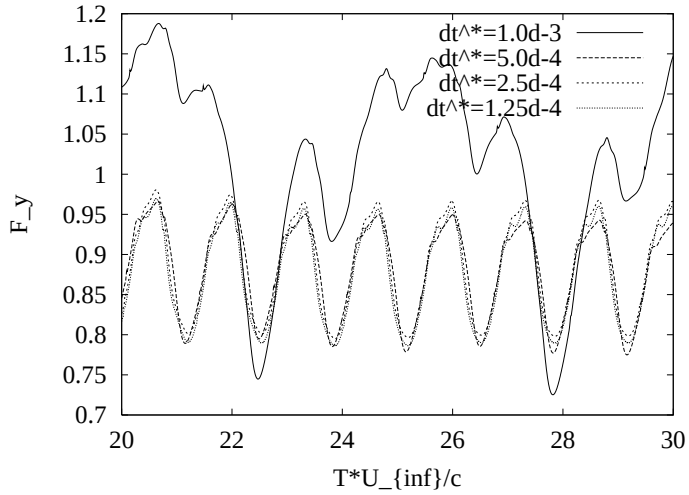

Figure 2: Time-step investigation, showing that a time-step below $5 \cdot 10^{-4}$ is needed in the active flow case to obtain a time independent solutions.

1.5 Results

Baseline investigation

The numerical solution is validated first by comparing with available measurements for the modified NACA-0015 airfoil, referred to as the Tel-Aviv University TAU-0015 airfoil, without jet actuation. A viscous no-slip boundary condition is imposed at the horizontal step, Figure 1, through which the jet is injected in the flow control cases. The computed flowfield without flow control is used as an initial condition for the computations with oscillatory blowing. All solutions were computed at $Re_c = 1.2 \bullet 10^6$.

RISOE experienced problems with the accurate prediction of the lift at high angles of attack for the passive case, see Figure 3. The computed results show a clear over-prediction for the stalled cases. This problem was initially also experienced by the other partner, FORTH, but was finally solved using a much higher grid density in the normal direction, see Figure 7. Using the k-ω SST model in the EllipSys2D code, the refinement of the mesh could not solve the problem with the over prediction. The FORTH results have been thoroughly described in ref [23] and [24].

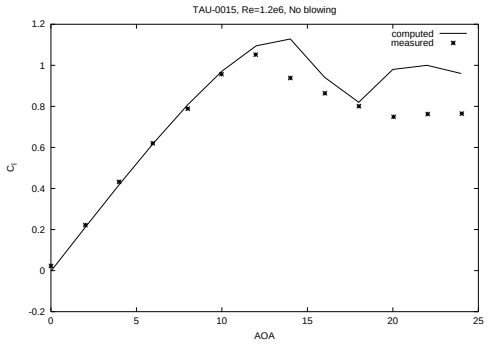

Figure 3: Comparison of computed lift and measured values, showing the RISOE results.

To give an impression of the detailed agreement of the results, the computed pressure distributions are shown in Figure 4, where the good agreement at angles of attack up to 12° is evident. At $\alpha = 12°$ the flow start to separate at the trailing edge of the airfoil, and for the two cases above this angle, $\alpha = 16°$ and 22°, over-prediction of the lift is observed, with the most severe case for the highest angle of attack.

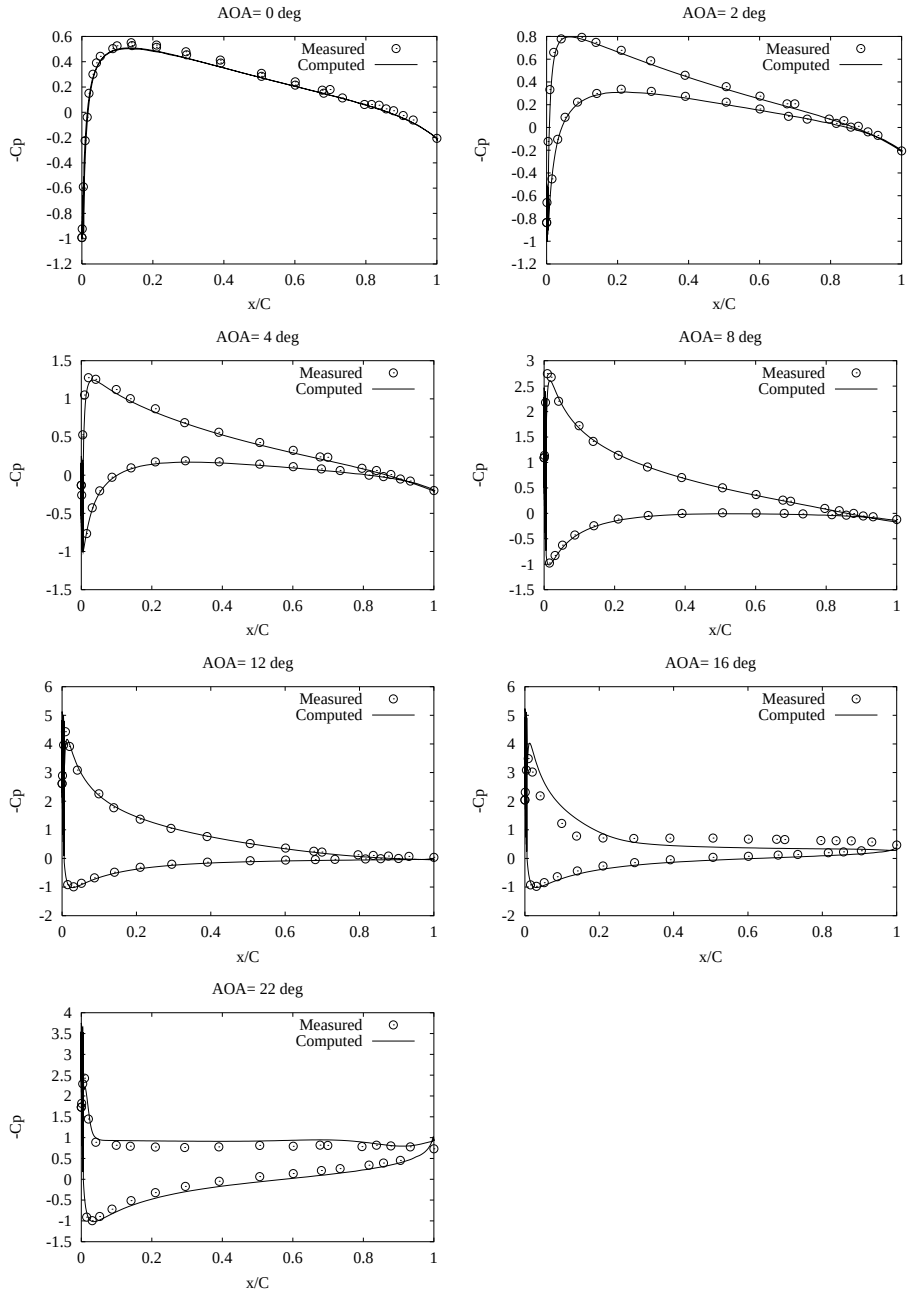

Figure 4: Pressure distributions for the TAU-0015 airfoil computed using the EllipSys2D code for the case of zero actuation.

Active flow cases

Following the initial passive flow computations, a series of cases using active flow control with pulsating jets are performed for stationary TAU-0015 airfoil. For the pulsating jet flow control, the TAU-0015 geometry implies jet exit velocities normal from the slot. The jet exit velocity V_J, which is non-dimensionalized with the free-stream and varies as $V_J(t)=V_a \cos(\omega_J t)$ where V_a is the amplitude and represents a zero net mass flux jet. Among the cases studied are cases with baseline values of control parameters of ref., $F^+=0.58$, $C_\mu=0.0003$ referred to as F1V1 in the following.

The parametric studies are performed by doubling the momentum coefficient C_μ and the frequency F^+. The case with doubled frequency and momentum coefficient is referred to

as F2V2, as the increase of C_μ can only be obtained by doubling the jet exit velocity, similar abbreviations are used for the other cases.

Both the baseline and the parametric study are performed for three angles of attack, 8°, 12° and 22°. The lift and drag for the baseline control values (F1V1) can be seen in Figure 7, showing an increased lift and nearly no change in the computed drag.

Both series of computations were able to qualitatively predict the effect of jet pulsation. Because of the improved agreement for the passive case, FORTH was even able to predict the correct amount of lift enhancement with applied flow control. FORTH performed a parametric investigation of the influence of the jet pulsation frequency and the momentum coefficient (jet exit velocity amplitude).

Looking at Figure 5 for $\alpha = 8°$, it can be seen that the application of flow control results in an increase of the mean lift and a reduction of the mean drag. The response of the lift is almost sinusoidal, while this is not the case for the drag. Additionally a small phase shift can be observed between the lift and the drag. Increase of the C_μ causes increase of the lift and drag oscillation amplitude, while an increase of the frequency results in a slightly higher mean value of the lift and a lower drag with a significantly smaller oscillation amplitude. It appears that for attached flow increase of the oscillation frequency has a beneficial effect. In contrast increase of the jet exit velocity does not appear to have a favourable net effect and in general causes an increase of the oscillation amplitude.

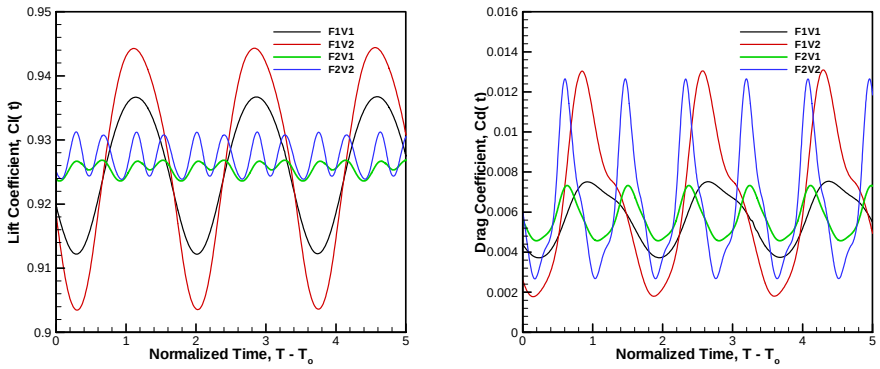

Figure 5: Load response with leading edge flow control for attached flow at $\alpha = 8^o$; Effect of pulsation frequency and jet exit velocity.

At $\alpha = 12°$ (see Figure 6) both lift and drag responses appear to have a higher harmonic content. Similarly to the fully attached case at 8°, an increase of the frequency appears to have a beneficial effect, while an increase of the jet exit velocity also in this case causes higher oscillation amplitudes. For the 22° case the behaviour is very similar to the previous two cases.

Figure 8 shows the RISOE computations of the F1V1 case at 22° compared to the passive computations. A small increase in lift is observed.

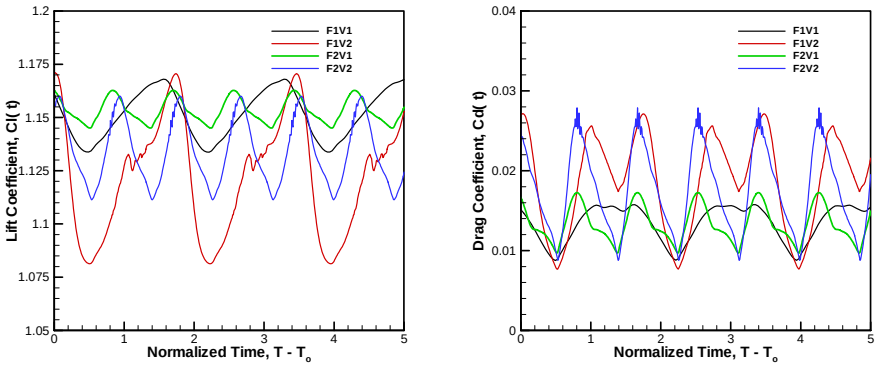

Figure 6: Load response with leading edge flow control for separated flow at $\alpha = 12^o$; Effect of pulsation frequency and jet exit velocity.

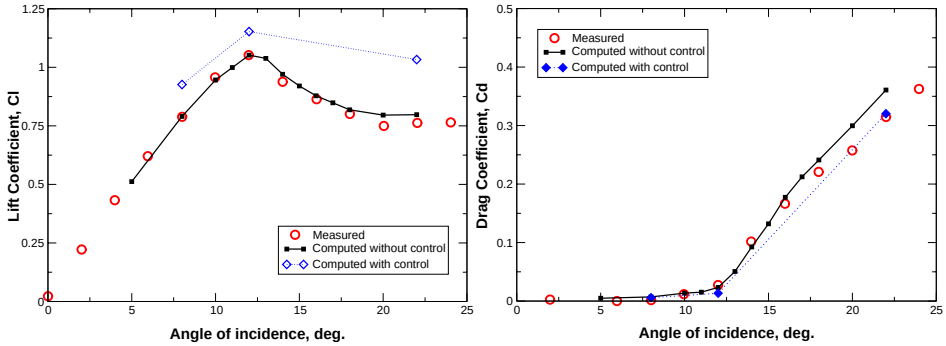

Figure 7: Comparison of computed and measured lift and drag for the passive case and the F1V1 active case, showing the computations by FORTH.

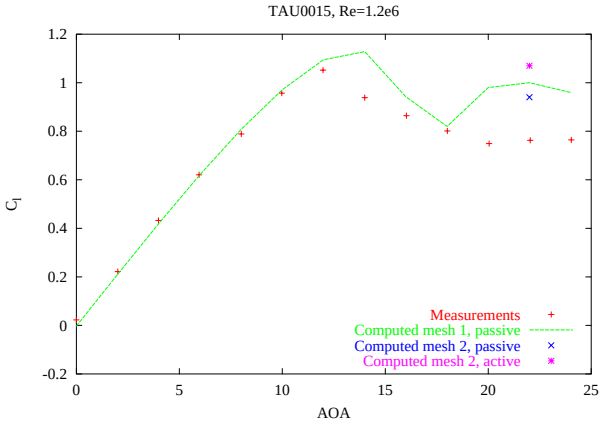

Figure 8: Comparison of the computed lift at 22° for the passive and active situation showing the RISOE results.

1.6 Discussions

Numerical investigation of pulsating jets has been performed. First agreement with measured lift and drag values were demonstrated for the passive case without any jet pulsation. The RISOE computations showed excellent agreement up to stall, followed by over-prediction of the lift, while the FORTH computations were able to capture the total lift curve. Following the initial passive computations, grid refinement and time-step dependency investigation were performed to establish the needs for the active computations. Finally, parametric computations were performed, varying the frequency and the jet exit velocity. The general trend is that increased frequency is beneficial, in that it reduces the oscillation amplitude and raises the mean lift level while lowering the mean drag level. An increased jet exit velocity has a tendency to increase the oscillation amplitude, which is not very attractive for load control on wind turbines.

2 Vortex Generators

Vortex generators are currently used to control the aerodynamic forces and increase the performance and predictability of some wind turbine rotors during operation. Finding the optimal chordwise position and spanwise spacing for vortex generators demands a lot of experimental investigations, which are expensive. The motivation for the present work is to develop models that can correctly predict the effect of vortex generators on airfoils and blades, which can help in the design phase, and thereby decrease the number of experiments performed. The delta wing shaped vortex generators are placed in an array of pairs on the suction side of the blade. See Figure 9.

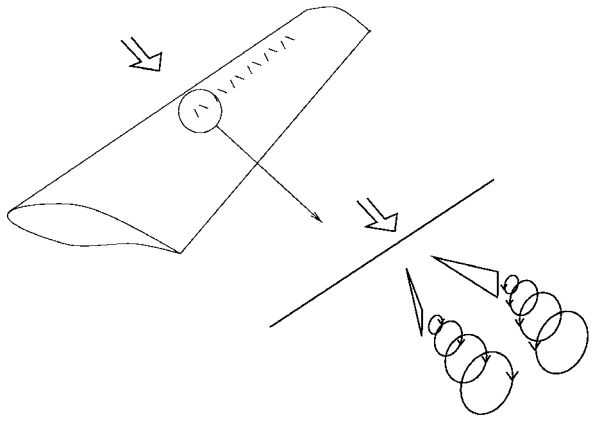

Figure 9: Schematic drawing showing the increased mixing due to vortex generators

When the flow passes the blade the vortex generators create a pair of counter rotating vortices, which transport momentum from the upper part of the boundary layer to the lower part of the boundary layer, and thereby increases the mixing closer to the wall. This leads to a fuller streamwise velocity profile and causes the boundary layer to better withstand the adverse pressure gradient and thereby delaying separation.

2.1 Methodology

Six partners are involved in the work. They are RISOE, CRES, DLR, DTU, VUB and LMG. Both RISOE and CRES are using phenomenological models, which can be used in 2D Navier-Stokes codes, while DLR, DTU and VUB are modelling the 3D vortex generator. The 3D work is described in ref.[25]. LMG is not making any computations.

RISOE method

The basic idea of the present model is to model stall delay effects of vortex generators by adding an extra source term to the turbulent kinetic energy equation of the turbulence model and thereby increases the production of turbulent kinetic energy to obtain a fuller streamwise velocity profile. Furthermore the model is developed for two-dimensional computations even though the flow around the vortex generator is highly three-dimensional. The CFD code EllipSys2D [20,21] and is used with the k-ω SST model for modeling turbulence.

The phenomenological vortex generator model suggested in the present study simulates the stall delay effect based on the assumption that the extra production of turbulent kinetic energy, P_k, based on dimensional analysis, is a function of the lift, L, of the

vortex generator. I.e. it is simply the lift of the vortex generator multiplied with a velocity scale, U_{tip}. U_{tip} is the velocity at the tip of the vortex generator. The model reads

$$P_k = c_1 L U_{tip} = c_1 \frac{1}{2} \rho U_{tip}^3 \pi \alpha_{VG} h_{VG} l_{VG} .$$

Here c_1 is an empirical constant and

$$L = C_l(\alpha_{VG}) \frac{1}{2} \rho U_{tip}^2 A_{VG} ,$$

where $C_l(\alpha_{VG}) = 2\ \pi\ \alpha_{VG}$ is a rough approximation of the lift coefficient of a small delta wing. (The deviation from $2\ \pi\ \alpha_{VG}$ is automatically included in the c_1 constant.) $A_{VG} = 1/2 \cdot h_{VG} l_{VG}$ is the projected area of the vortex generator. The model, which is based on integral parameters, gives the total extra production of turbulent kinetic energy, or the power generated by the vortex generator. I.e. P_k has the dimension [kg·m^2/s^3] or [W].

The extra production of kinetic energy is added in a volume representing the size of the vortex generated by the vortex generator. Here this volume is chosen to be a square with dimensions $2h_{VG}$x$2h_{VG}$ placed at the position of the vortex generator, see Figure 10

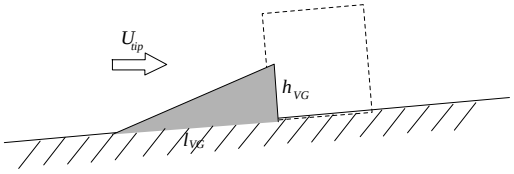

Figure 10: Schematic drawing showing the control volume definition of the vortex generator model.

The empirical constant c_1 has been calibrated to obtain the best overall agreement with respect C_l around $C_{l,max}$ i.e. at two angles of attack (α = 10° and 16° on the Risø-A1-18 airfoil) the flow was computed for various c_1 and the best overall agreement was obtained for c_1 = 0.6.

One advantage with this model is that the turbulent kinetic energy is a scalar and therefore only one equation needs to be modified.

The model was originally proposed by Hansen et al.[26] and has been further developed in Johansen et al.[27] and in the present project.

CRES method

CRES developed a phenomenological type model for VG's to be combined with an existing 2-D Navier-Stokes solution method[28]. In the context of the model, a two-dimensional boundary layer model and a system of co-rotating or contra-rotating vortex lines have been superposed to assemble the overall VG model, in the form of the average flow in the cross direction (pitch). Elementary incompressible flow theory for vortex flow has been employed to model the induced flow, which mainly affects the momentum conservation in the pitch direction and the turbulence production term of the turbulence equations. The model is summarized by the following source term

$$\mathbf{f(y)} = \begin{cases} \dfrac{1}{8\pi \mathbf{L}} \left(\dfrac{\Gamma}{\mathbf{y} - \mathbf{y_o}} \right)^2 \dfrac{\mathbf{y}}{\mathbf{y_o} - \mathbf{R_c}} & 0 \le \mathbf{y} \le \mathbf{y_o} - \mathbf{R_c} \\ -\dfrac{2}{3\mathbf{L}} \left(\dfrac{\Gamma}{\pi} \right)^2 \dfrac{1}{\mathbf{R_c^3}} (\mathbf{y} - \mathbf{y_o}) & \mathbf{y_o} - \mathbf{R_c} \le \mathbf{y} < \mathbf{y_o} + \mathbf{R_c} \\ -\dfrac{1}{8\pi \mathbf{L}} \left(\dfrac{\Gamma}{\mathbf{y} - \mathbf{y_o}} \right)^2 & \mathbf{y_o} + \mathbf{R_c} \le \mathbf{y} < \infty \end{cases} \quad (1)$$

that relies on to both the geometrical parameters related to the VG configuration the value of the circulation around the vortex line. In the present model, the circulation has been computed using simple Delta wing theory. The model distribution given by Equation (1) is plotted in Figure 11 for a vortex placed at y_o/C=1%. In turbulent flows, the production term augments by the vorticity of the vortex system.

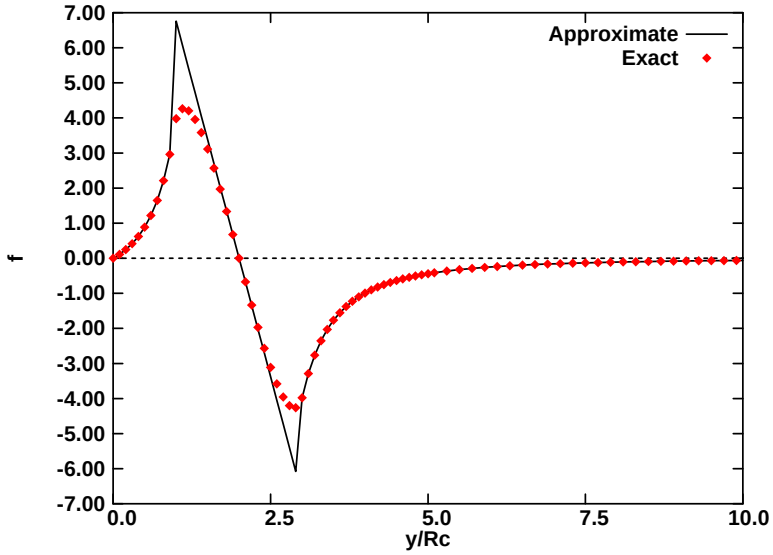

Figure 11: Model distributions of VGs.

In order to calibrate the VG model, the FFA-W3-241 airfoil test case was considered. Computations were compared with measurements from ref 30 with and without vortex generators. The calibration of the model was carried out in terms of the initiating and ending value of the vortex line radius (a linear distribution between the two values was assumed) and the actual value of the circulation. While Delta wing theory provides a value for this quantity, this was scaled down using an external coefficient k_c. From the numerical tests carried out in one VG configuration, the optimum value of k_c was 0.15. In the computations a single O-type mesh comprising 258x66 nodes, provided by RISOE, was used. In order to allow for a better resolution of the flow effects in the region that the vortex line was anticipated, extra grid lines were injected. Turbulence was approximated by means of the Menter's k-ω SST model.

2.2 Results

RISOE and CRES have computed lift and drag polars for three different airfoils; all with 6mm vortex generators placed at x/c = 0.20. These are Risø-A1-18, NACA 63-415 and FFA-W3-241. The latter was computed using four different vortex generator configurations. According to the test case definition computations were performed for

α = 0° to 30° at a Reynolds number of, *Re* = $1.6 \cdot 10^6$. Both smooth airfoil and airfoil equipped with vortex generators were computed.

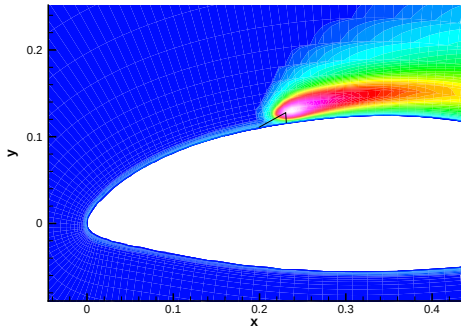

Figure 12: Contour plot of turbulent kinetic energy, Risø-A1-18, α = 10º, RISOE computation.

Figure 12 shows a contour plot of the turbulent kinetic energy of the flow around a Risø-A1-18 airfoil at an angle of attack of α = 10º computed using the RISOE vortex generator model. It is seen that the model generates extra turbulent kinetic energy, which causes the boundary layer to experience a delayed separation leading to a higher lift, as desired.

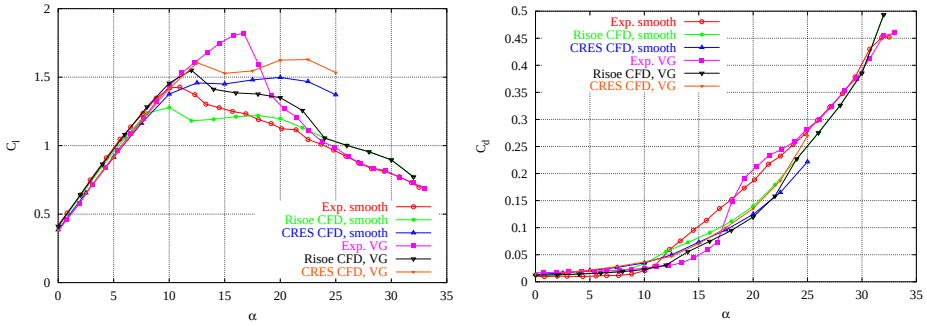

Figure 13: Computed C_l and C_d compared to measurement for the Risø-A1-18 airfoil

Figure 13 shows the C_l and C_d for the Risø-A1-18 airfoil. Both RISOE and CRES predict the smooth C_l and C_d fairly well up to stall. The RISOE computation predicts a too low maximum lift, while the CRES computation predicts a too high post stall lift. Adding the VG models delays stall and increase C_l as desired, but the amount of lift increase is not large enough.

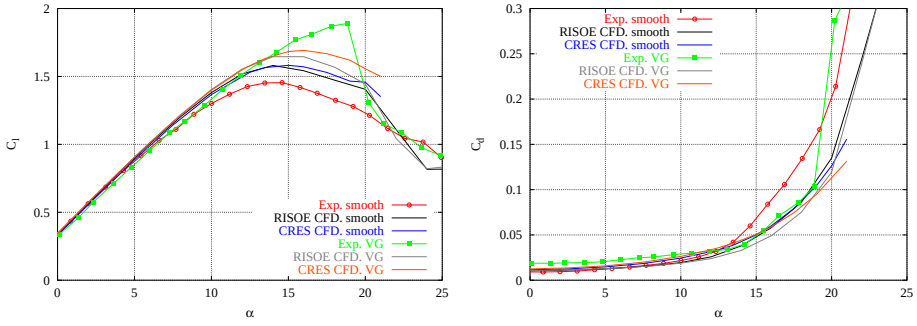

Figure 14: Computed C_l and C_d compared to measurement for the NACA 63-415 airfoil

Figure 14 shows the C_l and C_d for the NACA 63-415 airfoil. The agreement between the RISOE and CRES smooth computations are good but both deviate quite a lot from the measured values. Also for the VG computations the agreement between the two models is good but again the measurements are not well reproduced.

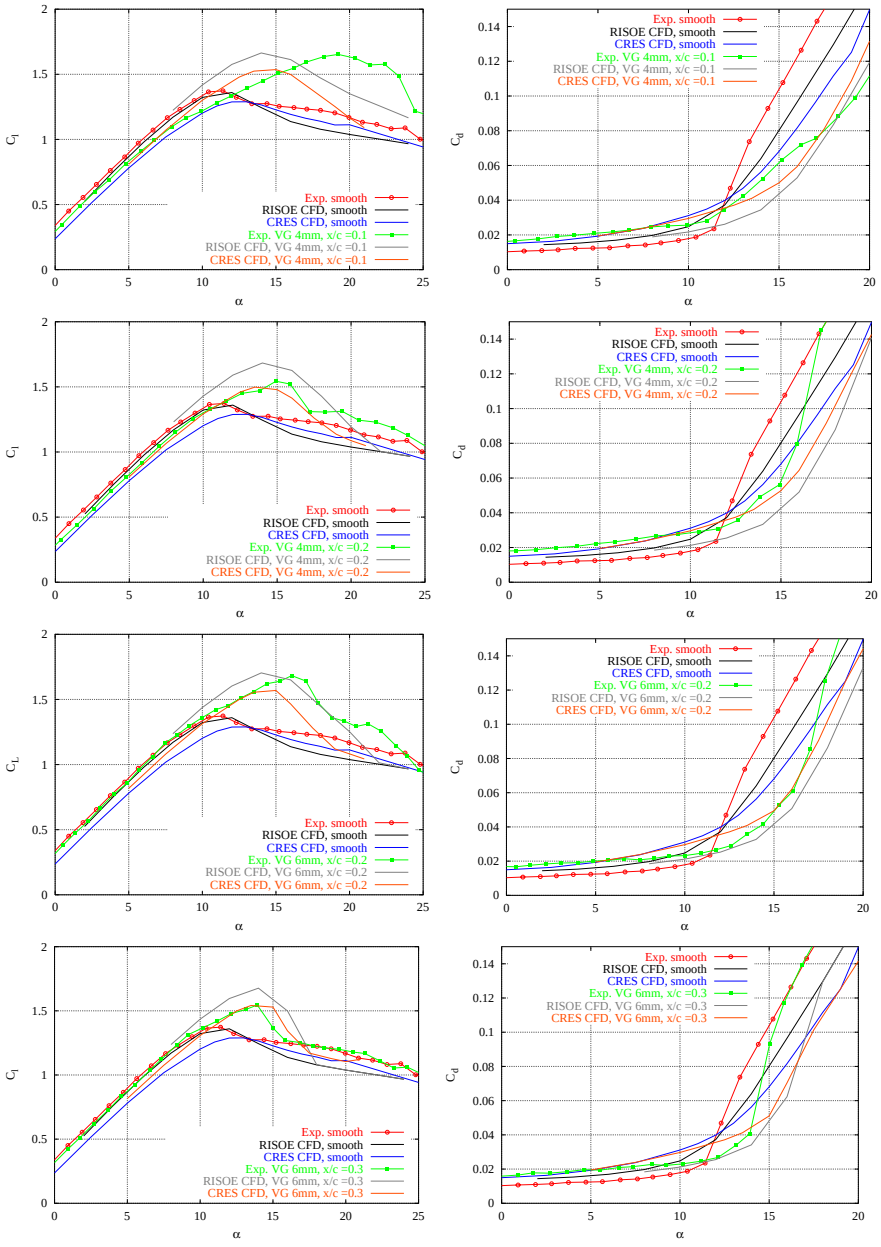

Figure 15:Computed C_l and C_d compared to measurement for the FFA-W3-241 airfoil

Finally, Figure 15 shows four vortex generator configurations on an FFA-W3-241 airfoil. The CRES smooth computations do not reproduce the smooth computations well; even in the linear region a large deviation is present. For the 4 mm VG placed at x/c = 0.1 the maximum lift is delayed to approximately α = 19º, which is not captured by any of the models. When the 4 mm VG is placed at x/c = 0.2 both models capture the correct maximum lift angle, but the RISOE model does not capture the correct lift level.

In general the CRES model results in lower C_l and higher C_d levels compared to the RISOE model.

2.3 Discussions

Two phenomenological vortex generator models have been developed by RISOE and CRES, respectively. The phenomenological models have been applied to three airfoil configurations, one of these with four different VG set-ups, and two with only one VG set-up. After performing the initial grid studies the clean configurations were computed.

The RISOE VG model was calibrated for one VG set-up at two different angles of attack for the FFA-W3-241 airfoil. Following this the VG model were applied to the remaining three VG set-ups for the FFA-W3-241 airfoil. Finally, the two additional airfoils were analyzed for a 6 mm VG placed on the suction side of the airfoil at x/chord=0.2.

Table 1 shows the error of the models defined as: One minus the increase in computed maximum lift coefficient compared to the measured increase in maximum lift coefficient. I.e. if perfect agreement is predicted using the models the error is 0 %. A 100% error corresponds to no improvements and –100 % error corresponds to 100% too much deviation. For all cases investigated the models shows qualitatively the correct behaviour, even though there are a considerable spread in the degree of success.

Table 1: Estimated error defined as 1-Increase in computed C_l compared to measured C_l using the phenomenological VG models of RISOE/DTU and CRES.

Airfoil	VG configuration	$1-\Delta Cl_{comp}/\Delta Cl_{meas.}$ RISOE	$1-\Delta Cl_{comp}/\Delta Cl_{meas.}$ CRES
FFA-W3-241	4 mm VG at x/c = 0.1	-7 %	12 %
FFA-W3-241	4 mm VG at x/c = 0.2	-88 %	-23 %
FFA-W3-241	6 mm VG at x/c = 0.2	-9 %	10 %
FFA-W3-241	6 mm VG at x/c = 0.3	-88 %	-54 %
Risø-A1-18	6 mm VG at x/c = 0.2	29 %	72 %
NACA 63-415	6 mm VG at x/c = 0.2	85 %	76 %

3 Stall Strips

Stall Strips serve the purpose of controlling the stall characteristics of a wind turbine blade both with respect to power and loads. The aim is to achieve smooth post stall behaviour such that undesirable stall induced vibrations are reduced, and at the same time minimising the drag penalty associated with the stall strip.

3.1 Methodology

Three partners are involved in the work. They are RISOE, CRES and LMG. RISOE and CRES are using their 2D Navier-Stokes codes. LMG is not making any computations. As defined in the test case definition the airfoil to be computed is the NACA 63-415, Re = 1.6 10^6, α = 0° to 30°. Four configurations were required. They are:

- Smooth airfoil
- 7mm stall strip placed at P-02.
- 7mm stall strip placed at P00.
- 7mm stall strip placed at P02.

The notation, P**, corresponds to the position of the stall strip placed at the stagnation point at the specific incidence angle, **. I.e. for P02 the stall strip is placed at the position of the stagnation point when α = 2°.

In the present project the stall strips are modelled by directly changing the surface of the surface description of the airfoils, see Figure 16.

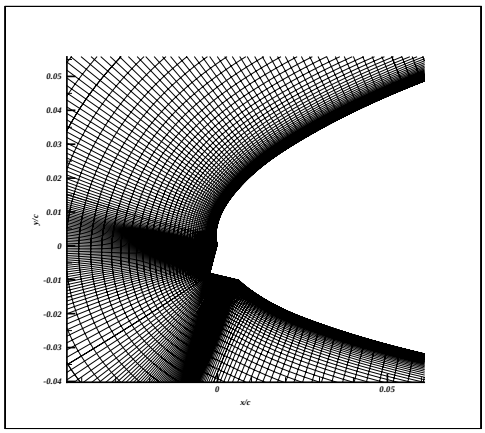

Figure 16: Example of a computational grid around an airfoil with stall strip placed at P02.

3.2 Results

RISOE Results

At RISOE a thorough study was made to investigate the capability of computing the flow around 2D airfoils fitted with stall strips. A thorough grid and time step dependence study has been carried out and six stall strip configurations together with a smooth configuration have been computed and compared with measurements. The complete work has been reported in[29].

Figure 17 shows a pressure contour plot of the flow around the NACA 63-415 airfoil with a stall strip placed at P00. A separation bubble above the stall strip is present, which causes a decrease in suction peak and eventually a lower lift.

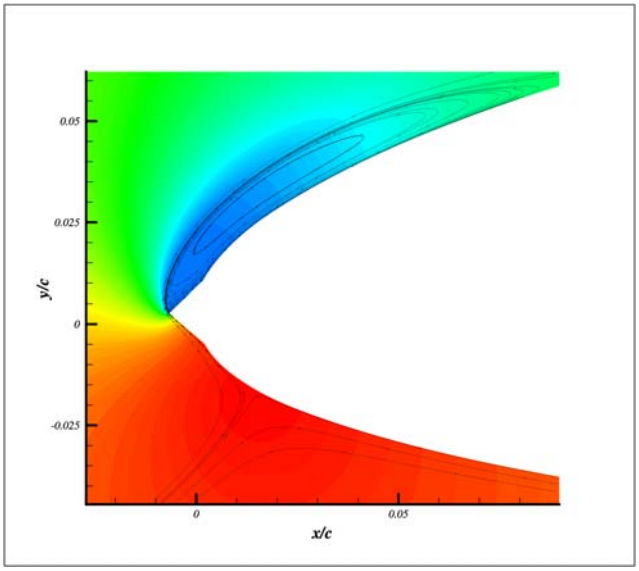

Figure 17: Pressure contour plot with streamlines, NACA 63-415, α = 12º, Stall strip at P00.

Figure 18 to Figure 20 show the lift and drag coefficient polars computed by RISOE for the three stall strip configurations.

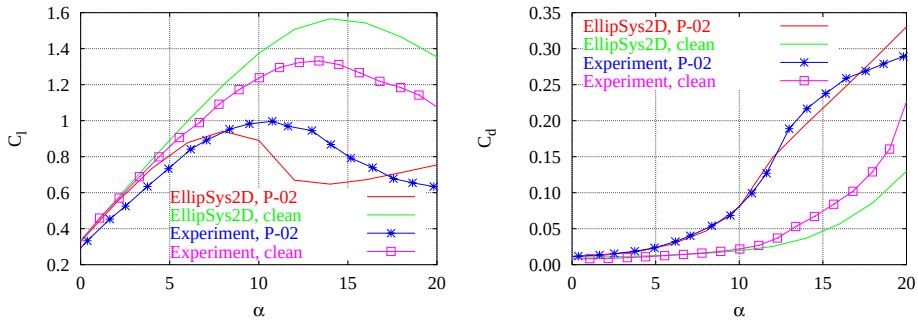

Figure 18: C_l and C_d for P-02

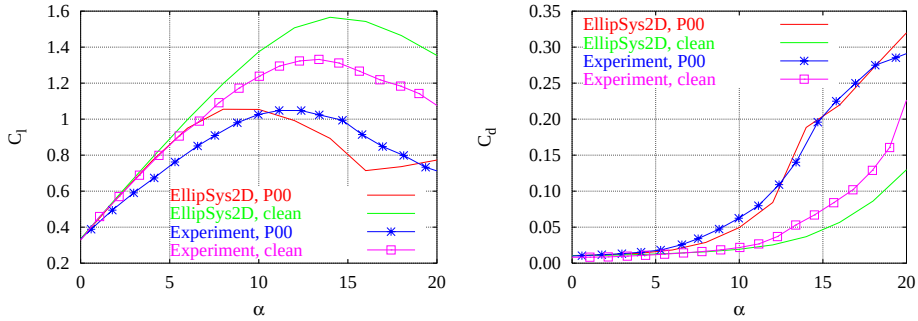

Figure 19: C_l and C_d for P00

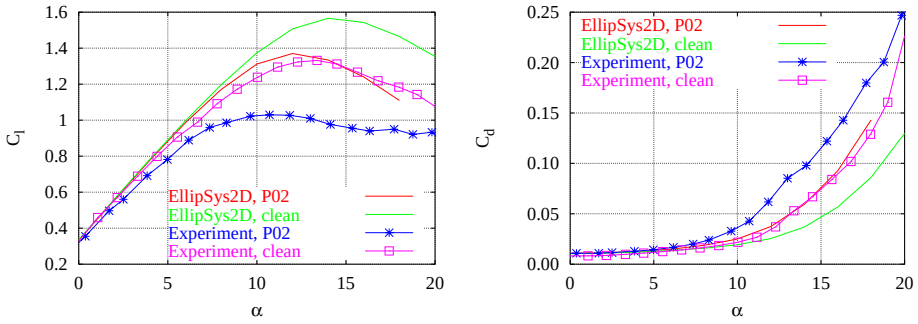

Figure 20: C_l and C_d for P02

CRES Results

Figure 21 to Figure 23 show the lift and drag coefficient polars computed by CRES for the three stall strip configurations.

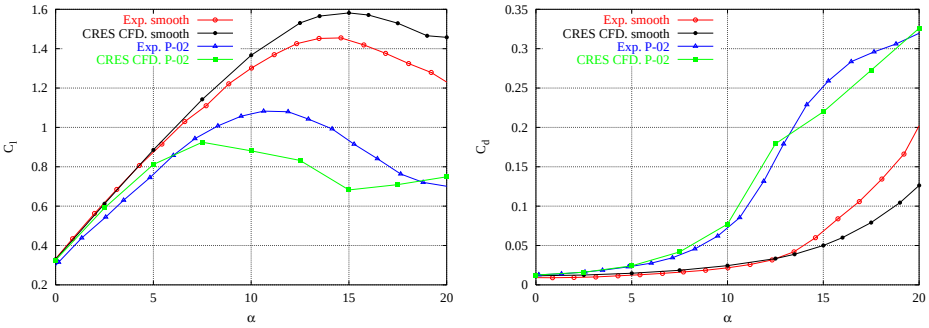

Figure 21 C_l and C_d for smooth and stall strip configuration P-02 (NACA-63-415 airfoil).

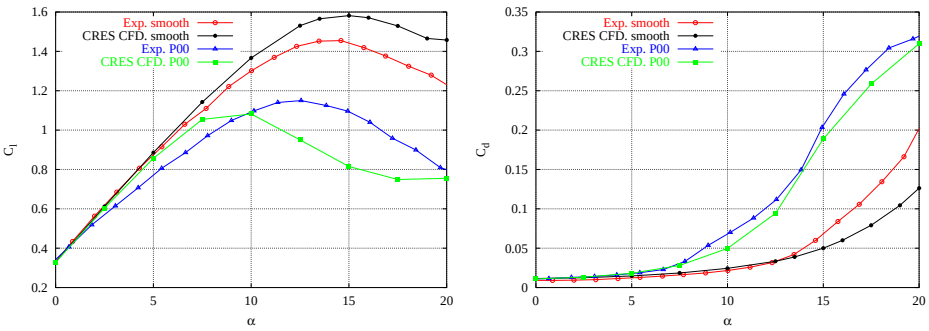

Figure 22 C_l and C_d for smooth and stall strip configuration P00 (NACA-63-415 airfoil).

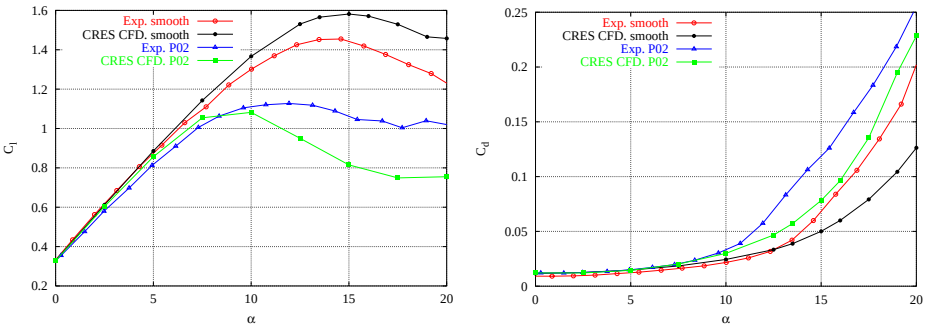

Figure 23 Lift and drag coefficient distributions for smooth and stall strip configuration P02 (NACA-63-415 airfoil).

After computing the NACA-63-415 airfoil it was decided that RISOE should compute the Risø-B1-18 airfoil with a stall strip placed at P02, due to the uncertainty of the NACA-63-415 measurements.

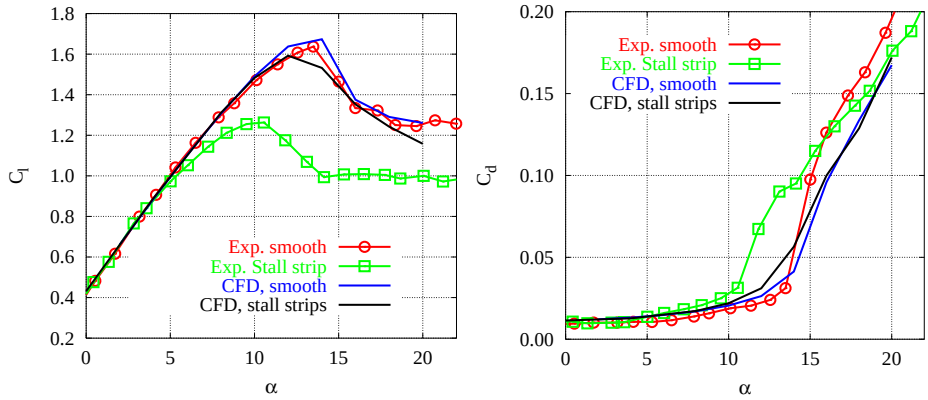

Figure 24 Lift and drag coefficient distributions for smooth and stall strip configuration P02 (Risø-B1-18 airfoil).

Figure 24 shows the RISOE results for the Risø-B1-18 airfoil and here the smooth computation is in much better agreement. But again the effect of modelling the stall strip is not successful.

3.3 Discussions

There was not sufficient agreement between the experimental results and the RISOE simulations to draw any conclusions of optimum position and geometry of the stall strip. The 7mm stall strips placed at P00 and P-02 had the greatest effect on the max lift followed by stall strip P02.

The mechanisms governing the flow properties of an airfoil fitted with stall strips are very complex, because it mostly depends on the nature of the l.e. separation bubble occurring downstream of the stall strip. Separation is one of the most multifaceted mechanisms to model numerically, and it is therefore likely that the flow is not accurately modelled with the current code. Furthermore, separation is a highly three-dimensional phenomenon, so a 2D model is possibly not sufficient to understand the physics of stall strip completely.

The NACA 63-415 airfoil was chosen as test case also for this investigation, and the problem of predicting even the smooth configuration would influence the conclusions. The computed results could therefore not directly be used to determine the optimum configuration for the stall strips, even though the computations qualitatively can predict the effect of the stall strips. To supplement the NACA-63-415 results it was decided that RISOE should make computations on the Risø-B1-18 airfoil. Here the smooth configuration was well predicted but the effect of the stall strip was not correctly predicted (See Table 2).

Table 2: Estimated error defined as 1-Decrease in computed Cl compared to measured Cl using stall strips.

Airfoil	SS configuration	$1-\Delta Cl_{comp}/\Delta Cl_{meas.}$ RISOE	$1-\Delta Cl_{comp}/\Delta Cl_{meas.}$ CRES
NACA 63-415	Stall strips at P-02	-74 %	-83 %
NACA 63-415	Stall strips at P00	-65 %	-61 %
NACA 63-415	Stall strips at P02	37 %	32 %
Risø-B1-18	Stall strips at P02	79 %	-

To get a better understanding of the behaviour of stall strip it is suggested that the stall strip are modelled in three dimensions, such that the true behaviour of the l.e. stall can be investigated. For such an investigation it would be necessary to employ Detached Eddy Simulation, in order to get significantly different results from the 2D calculations.

4 Roughness/Trip-tape

During operation a wind turbine blade will not always be perfectly smooth. This will alter the flow and it is necessary to take this into account during computations. Furthermore, the blade surface will eventually be contaminated with dirt, salt or bugs, which changes the surface and thereby the airfoil characteristics. Also roughness can be utilized to decrease some of the unattended unsteady effects and control the boundary layer by roughening the surface on strategic places. This roughness can e.g. assure that transition from laminar to turbulent flow is fixed and is independent of unsteady external conditions. It is therefore of large importance to be able to simulate these effects to obtain better and more physical predictions.

Various roughness models for non-smooth surfaces have been implemented.

4.1 Methodology

Four partners are involved in the work. They are RISOE, CRES, VUB and LMG. RISOE, CRES and VUB are using their 2D Navier-Stokes codes. LMG is not making any computations.

As defined in the test case definition the airfoils to be computed are the FFA-W3-241 and the Risø-A1-18 airfoils, Re = 1.6 10^6, α = 0° to 25°. The experimental data used for validation are taken from Fuglsang et al [30],[31]

The roughness chosen here is the 90 deg. Zig-zag tape, since the differences between the three types are very small. Two configurations were required.

They are:

- Smooth airfoil
- Roughness tape placed at x/c = 0.05 on suction side and x/c = 0.1 on pressure side.

RISOE and CRES method

RISOE and CRES use the roughness model developed by Wilcox[32], which is based on the k-ω turbulence model. k is the turbulent kinetic energy and ω is the specific dissipation rate. Here the roughness is included in the boundary condition for ω. On a rough wall ω is given by

$$\omega = \frac{u_\tau^2}{\nu} S_R, \quad u_\tau = \sqrt{\frac{\tau_w}{\rho}},$$

where ν is the kinematic viscosity, u_τ is the friction velocity, τ_w is the wall friction, ρ is the density and S_R is a non-dimensional coefficient given by

$$S_R = \begin{cases} \left(\frac{50}{k_s^+}\right)^2, & k_s^+ \le 25 \\ \left(\frac{100}{k_s^+}\right), & k_s^+ \ge 25 \end{cases} \qquad k_s^+ = \frac{k_s u \tau}{\nu}.$$

k_s^+ is the roughness height k_s made non-dimensional with u_τ and ν. Menters k-ω SST turbulence model[33] is based on Bradshaw's assumption for the SST limiter, which says that the turbulent kinetic energy is proportional to the Reynolds stress tensor. This is not

the case for a boundary layer above a rough wall. Hellsten and Laine[34] have suggested a revised version of the k-ω SST model which secures that the effect of roughness is modelled correctly using the Wilcox roughness model. Hellsten and Laine suggests that the turbulent viscosity, ν_t, is modelled using

$$\nu_t = \frac{a_1 k}{\max(a_1\omega; |\Omega| F_2 F_3)},$$

where a_1 is a model constant = 0.31, F_2 and F_3 are damping functions and Ω is the vorticity. The only difference from Menters version is an extra damping function F_3, which prevents Bradshaw's assumption to be activated in the sublayer, where it is not valid. F_3 is given by

$$F_3 = 1 - \tanh\left[\left(\frac{150\nu}{\omega y^2}\right)^4\right],$$

where y is the distance to the wall.

VUB method

Three computations are performed:

1. Smooth surface computed with the Spalart-Allmaras (S-A) turbulence model. The results hereafter named as "Smooth".
2. Fix the transition point at x/c=0.05 on the suction side and x/c=0.1 on the pressure side, and use the transition model in Euranus together with S-A one equation model. The results hereafter named as "Transition"
3. Directly mesh the roughness geometry as shown in Figure 25. The results hereafter named as "Trip Geom". Both the S-A model and linear k-ε model are used. It is found that the C_p computed with the two models are closely the same at α = 4º, 8º and 12º for the Risø-A1-18 airfoil. Hence, shown are only the data computed with the k-ε model.

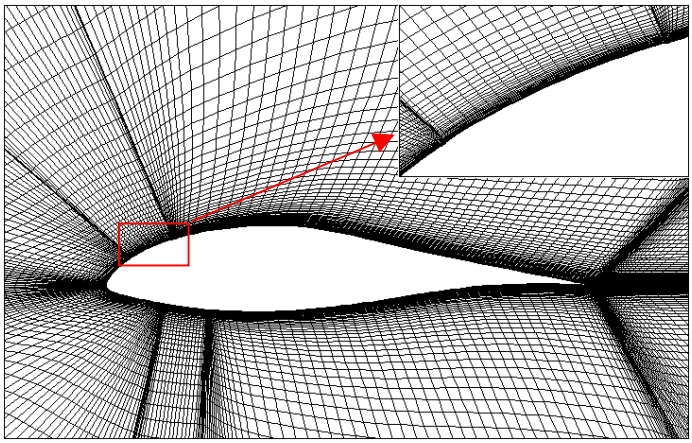

Figure 25: Mesh around the Risø-A1-18 airfoil where the roughness tape is directly modelled as a deviation of the surface geometry.

4.2 Results

RISOE Results

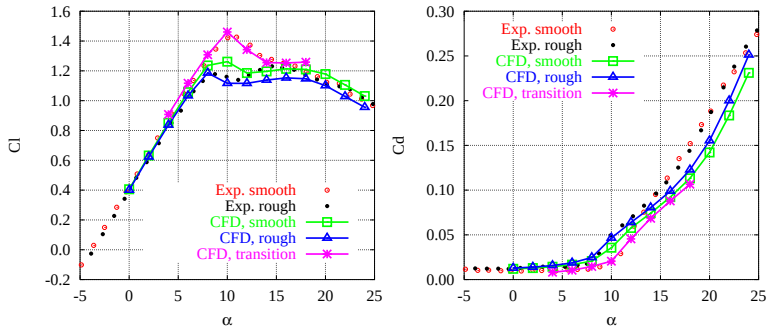

Figure 26: Risø-A1-18 airfoil. RISOE computations of roughness tape placed at x/c = 0.05 on suction side and x/c = 0.1 on pressure side.

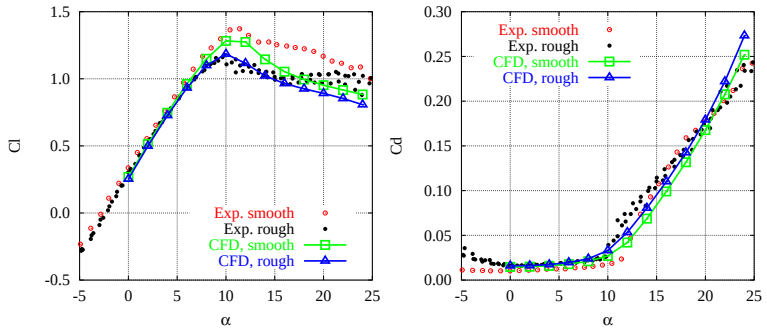

Figure 27: FFA-W3-241 airfoil. RISOE computations of roughness tape placed at x/c = 0.05 on suction side and x/c = 0.1 on pressure side.

The fully turbulent flow computation, denoted as *CFD, smooth*, showed for the Risø-A1-18 airfoil that it is necessary to include transition to properly predict the airfoil characteristics on the smooth airfoil. This was not the case for the FFA-W3-241 airfoil. Employing the roughness model good agreement with measurements is obtained.

CRES Results

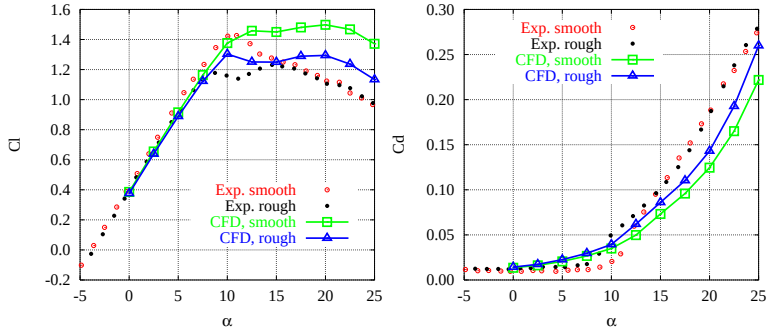

Figure 28: Risø-A1-18 airfoil. CRES computations of roughness tape placed at x/c = 0.05 on suction side and x/c = 0.1 on pressure side.

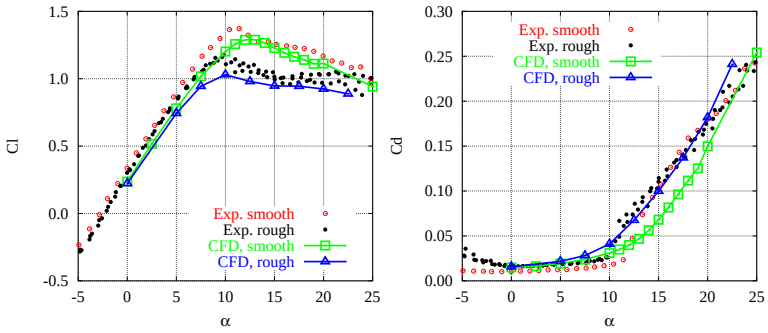

Figure 29: FFA-W3-241 airfoil. CRES computations of roughness tape placed at x/c = 0.05 on suction side and x/c = 0.1 on pressure side.

VUB Results

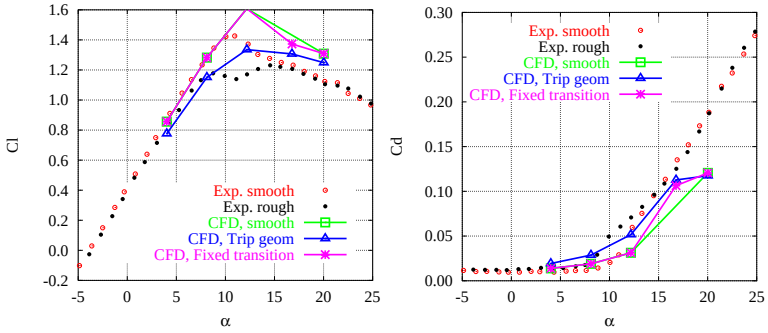

Figure 30: Risø-A1-18 airfoil. VUB computations of roughness tape placed at x/c = 0.05 on suction side and x/c = 0.1 on pressure side.

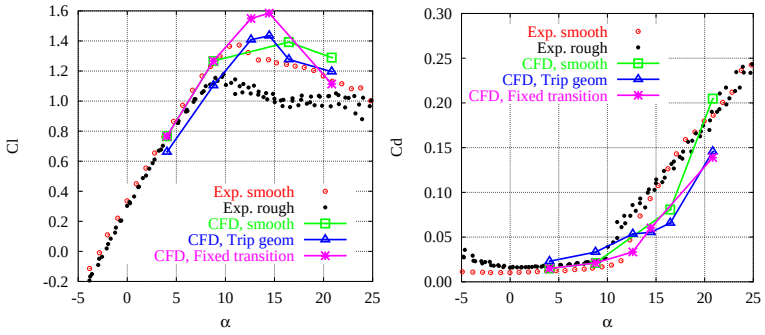

Figure 31: FFA-W3-241 airfoil. VUB computations of roughness tape placed at x/c = 0.05 on suction side and x/c = 0.1 on pressure side.

4.3 Discussions

Three partners have been involved in modelling roughness on airfoil flows. RISOE and CRES have employed a roughness model, while VUB has physically modelled the trip tape by changing the surface geometry. The RISOE results indicate that it is necessary to use a transition prediction model to properly predict the lift and drag coefficients on the smooth Risø-A1-18 airfoil. Employing a roughness model the agreement with measurements is quite good, where both maximum lift and post-stall behaviour is well predicted. The large error of the FFA-W3-241 (see Table 3) is caused by the misprediction of maximum lift on the smooth airfoil.

The CRES results on the Risø-A1-18 airfoil show an over prediction of lift in the post stall area but the relative decrease near maximum lift using a roughness model is well predicted. Better agreement is observed on the FFA-W3-241 airfoil even though the maximum lift is not well captured.

The VUB results do not predict the correct maximum lift for either of the smooth airfoils. Employing roughness gives the correct trend but quantitatively not the correct level of lift or drag. The estimated errors are shown in Table 3.

Table 3: Estimated error defined as 1-decrease in computed C_l compared to measured C_l using roughness.

Airfoil	**Roughness configuration**	**1-$\Delta Cl_{comp}/\Delta Cl_{meas.}$ RISOE**	**1-$\Delta Cl_{comp}/\Delta Cl_{meas.}$ CRES**	**1-$\Delta Cl_{comp}/\Delta Cl_{meas.}$ VUB**
Risø-A1-18	x/c = 0.05 on s.s & x/c = 0.10 on p.s.	12 %	-36 %	12 %
FFA-W3-241	x/c = 0.05 on s.s & x/c = 0.10 on p.s.	53 %	30 %.	-25 %

5 Conclusions

In the EC project KNOW-BLADE a work package has been defined to investigate the possibility to numerically model aerodynamic accessories in existing Navier-Stokes solvers. Four different aerodynamic accessories have been investigated in the present report.

Firstly, the potential of applying active flow control by means of a pulsating jet placed at the leading edge in order to enhance lift without increasing drag too much. The general trend is that increased pulsation frequency is beneficial, in that it reduces the oscillation amplitude and raises the mean lift level while lowering the mean drag level. An increased jet exit velocity has a tendency to increase the oscillation amplitude, which is not very attractive for load control on wind turbines.

Secondly, the effect of vortex generators has been modelled using two phenomenological vortex generator models developed by RISOE and CRES. The phenomenological models have been applied to three airfoil configurations, one of these with four different vortex generator set-ups, and two with only one vortex generator set-up. For all cases investigated the models shows qualitatively the correct behaviour, even though there are a considerable spread in the degree of success.

Thirdly, the influence of adding a stall strip for changing the airfoil characteristics was investigated. Stall strips at three different positions were directly modelled by changing the airfoil geometry. In general the 7mm stall strips placed at P00 and P-02 had the greatest effect on the max lift followed by stall strip P02. Unfortunately, there was not sufficient agreement between the experimental results and the simulations to draw any conclusions of optimum position and geometry of the stall strip.

Finally, the effect of surface roughness was modelled by either modifying the boundary condition of the specific dissipation rate, ω, in the k-ω SST turbulence model or by modifying the airfoil geometry. Both methods gave the correct trend, i.e. decreasing maximum lift. Using the modified turbulence model gave better agreement with roughness measurements compared to the approach of modifying the airfoil geometry. VUB was not able to correctly predict maximum lift even in the smooth case.

In general, it must be concluded that the flow around a 2D airfoil section with aerodynamic accessories is quite complex and eventually three-dimensional and the investigated models does not satisfactorily predict the effects of applying these accessories. It must be concluded that to get a better understanding of the behaviour of adding aerodynamic accessories, these must be modelled in three dimensions so that the real physical phenomena can be simulated. This will demand more advanced turbulence models such as Detached Eddy Simulation or Large Eddy Simulation models to be employed.

6 Acknowledgement

The work was carried out under a contract with the EC, ENK6-CT-2001-00503, KNOW-BLADE. Computations by RISOE were made possible by the use of the IBM RS6000 SP at Risø central computing facility and the Danish Centre for Scientific Computing Linux cluster Yggdrasill facility in Lyngby, Denmark.

References

[1] Chandrasekhara, M. S., Wilder, M. C., and Carr, L. W., 1999. “Compressible dynamic stall control using a shape adaptive airfoil”'. AIAA Paper 99--0650.

[2] Chandrasekhara, M. S., Wilder, M. C., and Carr, L. W., 1999. “Compressible dynamic stall control: a comparison of different approaches”. AIAA Paper 99--3122.

[3] Chang, R. C., Hsiao, F. B., and Shyu, R. N., 1992. “Forcing level effects of internal acoustic excitation on the improvement of airfoil performance”'. AIAA Journal, 29 (5) pp. 823--829.

[4] Greenblatt, D., Nishiri, B., Dabari, A., and Wygnanski, I., 1999. “Some Factors Affecting Stall Control with Particular Emphasis on Dynamic Stall”. AIAA Paper 99--3504.

[5] Greenblatt, D. and Wygnanski, I., 1999. “Parameters affecting dynamic stall control by oscillatory excitation”. AIAA Paper 99--3121.

[6] Seifert, A., Bachar, T., Koss, D., Shepshelovich, M., and Wygnanski, I., 1993. “Oscillatory blowing a tool to delay boundary--layer separation”. AIAA Journal, 31 (11) pp. 2052--2060.

[7] Seifert, A. and Pack, L. G., 1999. “Oscillatory control of separation at high Reynolds numbers”. AIAA Journal, 37 (9) pp. 1062--1079.

[8] Weaver, D., McAllister, K. W., and Tso, J., 1998. “Suppression of dynamic stall by steady and pulsed upper—surface blowing”. AIAA Paper 98--2413.

[9] Rao, J. L., Ko, G. J., Strganac, T., and Rediniotis, O. K., 2000. “Flow separation control via synthetic jet actuation”. AIAA Paper 2000--0407.

[10] McCormick, D. C., 2000. “Boundary layer separation control with directed synthetic jets”. AIAA Paper 2000--0519.

[11] Smith, B. L. and Glezer, A., 1988. “The Formation and Evolution of Synthetic Jets”. Physics of Fluids, 10 (9) pp. 2281--2297.

[12] Gad--el--Hak, M. and Bushnell, D. M., 1991. “Separation Control: Review”. Journal of Fluids Engineering, 113 (5) pp. 5--30.

[13] Weaver, D., McAllister, K. W., and Tso, J., 1998. “Suppression of dynamic stall by steady and pulsed upper—surface blowing”'. AIAA Paper 98--2413.

[14] Wu, J. M., Lu, X. Y., and Wu, J. Z., 1997. “Post--stall lift enhancement on an airfoil by local unsteady control, part ii. mode competition and vortex dynamics”. AIAA Paper 97--2046.

[15] Hassan, A. A. and JanakiRam R. D., 1997. “Effects of zero--mass synthetic jets on the aerodynamics of the NACA--0012 airfoil”. AIAA Paper 97--2326.

[16] Hassan, A. A., 1998. “Numerical simulations and potential applications of zero-mass jets for enhanced rotor aerodynamic performance”. AIAA Paper 98--0211.

[17] Donovan, J. F., Kral. L. D., and Cary, A. W., 1998. “Active control applied to an airfoil”. AIAA Paper 98--0210.

[18] Ekaterianris, J. A., 2002. ``Numerical investigation of dynamic stall active control of incompressible and compressible flows". Journal of Aircraft, 39 (1) pp. 71-78.

[19] Ekaterinaris, J. A., 1998. Numerical simulation of incompressible two--blade rotor flowfields". Journal of Propulsion and Power, 14 (3) pp. 367--374.

[20] Michelsen J.A., ”Basis3D - a Platform for Development of Multiblock PDE Solvers” Technical Report AFM 92-05, Technical University of Denmark, 1992.

[21] Michelsen J.A., ”Block structured Multigrid solution of 2D and 3D elliptic PDE's”, Technical Report AFM 94-06, Technical University of Denmark, 1994.

[22] Sørensen N.N., ”General Purpose Flow Solver Applied to Flow over Hills”, Risø-R-827-(EN), Risø National Laboratory, Roskilde, Denmark, June 1995.

[23] Ekaterinaris J.A. “Active Flow Control of Wing Separated Flow”, 2003 4th ASME/JSME Joint Fluids Engineering Conference, July 6-10, 2003, Honolulu, Hawaii, USA.

[24] Ekaterinaris J.A. “Prediction of Active Flow Control Performance on Airfoils and Wings” Accepted for publication in ??

[25] Johansen J., Sørensen N.N. et al. “KNOW-BLADE Task3 report; Rotor Computations with Aerodynamic Accessories”, To be published as a Risø-R report.

[26] Hansen M.O.L., Westergaard, C. ”Phenomenological Model of Vortex Generators”. IEA, Aerodynamics of Wind Turbines, 9th Symposium, Stockholm, December 11-12, 1995

[27] Johansen, J., Sørensen N.N., Hansen M.O.L.”CFD vortex generator model”. European Wind Energy Conference 2001, 2-6 July 2001, Copenhagen, Denmark.

[28] Politis E.S., Nikolaou I.G and Chaviaropoulos P.K “Phenomenological modelling of vortex generators”, European Wind Energy conference, EWEC 2003, 16-19 June 2003, Madrid, Spain.

[29] Zahle, F., Sørensen N.N., Johansen, J. ”CFD Study of a NACA 63-415 Aerofoil Fitted with Stall Strips”, Risø-R-1370(EN), September, 2002.

[30] Fuglsang P., Antoniou I., Dahl K.S., Madsen H.A. ”Wind Tunnel Tests of the FFA-W3-241, FFA-W3-301 and NACA63-430 Airfoil”, Risø-R-1041(EN), Risø National Laboratory, Denmark, December, 1998.

[31] Fuglsang P., Dahl K., Antoniou I. ”Wind Tunnel Tests of the Risø-A1-18, Risø-A1-21 and Risø-A1-24 Airfoils”, Risø-R-1112(EN), Risø National Laboratory, Denmark, June, 1999.

[32] Wilcox, D.C. ”Turbulence Modeling for CFD”, DCW Industries, Inc.,1993.

[33] Menter, F. R. ”Zonal Two Equation k-ω Turbulence Models for Aerodynamic Flows”, AIAA Paper 93-2906, 1993.

[34] Hellsten, A. and Laine, S: ”Extension of the k-ω SST Turbulence Model for Flows over Rough Surfaces”. AIAA Paper 97-3577-CP, 1997.

Mission

To promote an innovative and environmentally sustainable technological development within the areas of energy, industrial technology and bioproduction through research, innovation and advisory services.

Vision

Risø's research **shall extend the boundaries** for the understanding of nature's processes and interactions right down to the molecular nanoscale.

The results obtained shall **set new trends** for the development of sustainable technologies within the fields of energy, industrial technology and biotechnology.

The efforts made **shall benefit** Danish society and lead to the development of new multi-billion industries.